Calibrationless Parallel Imaging Reconstruction for Multi-slice MR Data using Low-Rank Tensor Completion

Yilong Liu[1,2], Zheyuan Yi[1,2,3], Yujiao Zhao[1,2], Fei Chen[3],

Yanqiu Feng[4], Hua Guo[5], Alex T. L. Leong[1,2], and Ed X. Wu[1,2*]

[1]Laboratory of Biomedical Imaging and Signal Processing, the University of Hong Kong, Hong Kong SAR, People's Republic of China

[2]Department of Electrical and Electronic Engineering, the University of Hong Kong, Hong Kong SAR, People's Republic of China

[3]Department of Electrical and Electronic Engineering, Southern University of Science and Technology, Shenzhen, People's Republic of China

[4]School of Biomedical Engineering, Southern Medical University, Guangzhou, People's Republic of China

[5]Center for Biomedical Imaging Research, Department of Biomedical Engineering, Tsinghua University, Beijing, People's Republic of China

[*]Correspondence to:

Ed X. Wu, Ph.D.
Department of Electrical and Electronic Engineering
The University of Hong Kong, Hong Kong SAR, China
Tel: (852) 2859-7096
Fax: (852) 2559-8738
Email: ewu@eee.hku.hk

Short Running Title: Multi-slice Reconstruction with Low-Rank Tensor Completion

Total Word Count: 4400 words in main text + 9 figures + 1 table

Keywords: Multi-slice, parallel imaging, low-rank, Hankel tensor completion

Liu Y, Yi Z, Zhao Y, Chen F, Feng Y, Guo H, Leong ATL, Wu EX. Calibrationless parallel imaging reconstruction for multislice MR data using low-rank tensor completion. Magn Reson Med. 2021 Feb;85(2):897-911. doi: 10.1002/mrm.28480.

Abstract

Purpose: To provide joint calibrationless parallel imaging reconstruction of highly accelerated multi-slice 2D MR k-space data.

Methods: Adjacent image slices in multi-slice MR data have similar coil sensitivity maps, spatial support, and image content. Such similarities can be utilized to improve image quality by reconstructing multiple slices jointly with low-rank tensor completion. Specifically, the multi-channel k-space data from multiple slices are constructed into a block-wise Hankel tensor, and iteratively updated by promoting tensor low-rankness through high-order SVD (HOSVD). This multi-slice block-wise Hankel tensor completion (MS-HTC) was implemented for 2D spiral and Cartesian k-space undersampling where sampling patterns vary between adjacent slices. The approach was evaluated with human brain MR data, and compared to the traditional single-slice simultaneous autocalibrating and k-space estimation (SAKE) reconstruction.

Results: The proposed MS-HTC approach robustly reconstructed highly undersampled multi-slice 2D spiral and Cartesian data. It produced substantially lower level of artifacts compared to the traditional single-slice SAKE reconstruction. Quantitative evaluation using error maps and root mean-square-errors (RMSEs) demonstrated its significantly improved performance in terms of residual artifacts and RMSE.

Conclusion: Our proposed MS-HTC method exploits the similar coil sensitivity and image content within multi-slice MR data through a tensor completion framework. It offers a new and effective approach to acquire and reconstruct highly undersampled multi-slice MR data in a calibrationless manner.

Introduction

Parallel imaging is widely used in clinical MRI to accelerate data acquisition[1,2] or compensate acquisition imperfections[3,4]. However, artifacts and noise amplification can become severe with high undersampling or acceleration factor. Moreover, conventional parallel imaging methods need coil sensitivity calibration information obtained from additional calibration scan[1] or autocalibrating signals (ACS)[2]. Acquiring calibration data can further prolong the acquisition. Mismatch between calibration data and undersampled data due to subject motion[2,5] or geometrical distortion[6] can undermine the reconstructed images in terms of residual artifacts and SNR. In spiral imaging, acquiring sufficient ACS data prolongs the acquisition window, which can lead to blurring and artifacts due to off-resonance effect.

In a typical multi-slice clinical scan, multiple consecutive 2D slices are acquired to provide a volume coverage. Adjacent slices often exhibit similar image content due to slow structural variations along slice direction, especially when the slice thickness/gap is sufficiently small[7]. Such information has been explored for estimating the unacquired k-space data by interpolating data from other slices[8-10]. The similarity can also present as sparsity of difference between adjacent slices[7]. In this regard, the difference between adjacent slices can be treated as a sparse transform, and then utilized for compressed sensing based super-resolution reconstruction. With adjacent slices being sufficiently thin and undersampled differently, the multi-slice data can be sparse in a properly chosen transform domain, which offers unique advantages in recovering coarse-scale component and makes multi-slice reconstruction superior to single-slice reconstruction[11]. However, these earlier approaches do not utilize the multi-channel information, which is now widely available in clinical scans.

On the other hand, the coil sensitivity varies smoothly within the image planes and along slice direction, and adjacent slices have different but similar coil sensitivity maps[12-14]. Therefore, it is feasible to acquire calibration data only for a few evenly spaced slices, and then linearly interpolate GRAPPA weights for other slices from those for the adjacent slices[13]. Alternatively, different slices can have an interleaved sampling pattern, such that the calibration data can be obtained by combining the central k-space lines from adjacent slices[13]. This is conceptually similar to TGRAPPA, where the

calibration data are combined from adjacent time frames[15]. These two approaches require very little or no additional calibration data by exploiting the coil sensitivity similarity among adjacent slices.

The aforementioned approaches of exploring coil sensitivity and image content similarities among adjacent slices can be incorporated with calibrationless parallel imaging reconstruction. In recent years, low-rank matrix completion has made it possible to perform calibrationless reconstruction, which inherently explores the redundant information in k-space[16-20]. Simultaneous autocalibrating and k-space estimation (SAKE) formulates parallel imaging as a low-rank matrix completion problem, implicitly utilizing the data redundancy from multi-channel acquisition and limited spatial support[16]. LORAKS[17] exploits the limited spatial support and smooth phase of MR images, and has been extended for multi-channel parallel imaging reconstruction (P-LORAKS[18]). ALOHA formulates the transform sparsity by annihilating filter-based low-rank Hankel matrix completion[19,20]. These methods can also be adapted for Nyquist ghost elimination in EPI reconstruction by treating EPI data from different readout polarities/shots as from different virtual channels[19,21-23]. The central k-space of multiple slices can also be recovered jointly by extending the existing low-rank matrix completion methods with tensorial expressions, and used as calibration data for subsequent parallel imaging reconstruction[12].

The multi-slice nature of 2D acquisition allows different slices having complementary sampling pattern, and enables missing k-space sample estimation from adjacent slices. For example, a sampling scheme that has varying sampling density across different slices can be adopted, and missing data from slices with extremely sparse sampling can be interpolated from its adjacent slices which are more densely sampled[8,24]. Randomizing the sampling patterns of adjacent slices can improve the incoherency between slices when multiple slices are reconstructed together with compressed sensing methods[11,25].

In this study, we propose to jointly reconstruct multiple adjacent slices through a block-wise Hankel tensor completion framework (MS-HTC). The proposed approach exploits the coil sensitivity maps, spatial support, and image content similarities among adjacent slices. It is further enhanced by using complementary sampling patterns across difference slices. The proposed approach was implemented for both multi-slice spiral

and Cartesian imaging, and evaluated with multi-slice human brain MR data.

Methods

Structured low-rank multi-channel multi-slice tensor

The proposed approach exploits correlations of multi-channel multi-slice k-space data by structuring the k-space data into a block-wise Hankel tensor. As shown in **Figure 1**, k-space data from each slice are structured into a block-wise Hankel matrix of which columns are vectorized blocks from sliding kernels across the entire k-space[16], and then stacked along a third dimension, forming a 3rd-order tensor, termed as multi-slice tensor (***T***). Its three dimensions corresponding to the k-space samples from different kernels, channels (while within a kernel), and slices are termed as kernel, channel, and slice dimensions, respectively. The multi-slice tensor can be viewed as a 3-way tensor by unfolding the tensor into matrices[26,27]. Specifically, the multi-slice tensor can be unfolded by stacking vectors of its kernel, channel, or slice dimensions, which are termed as 1-mode, 2-mode, and 3-mode unfolding, with the matrix unfolding representations denoted as $T_{(1)}$, $T_{(2)}$, and $T_{(3)}$, respectively.

As revealed in auto-calibrating parallel imaging reconstruction, each k-space sample can be fitted from its neighborhood within a compact kernel, which should be consistent across the whole k-space[2,28]. This implies that the block-wise Hankel matrix should be inherently low-rank[16]. Due to the similarities in coil sensitivity, spatial support, and image content across adjacent slices, the multi-slice tensor is more rank-deficient when compared to the block-wise Hankel matrix constructed from a single slice. First, different slices have similar image content, which has been used to interpolate the missing samples from its adjacent slices, with the weights estimated from the central k-space[8,29]. This can be interpreted as explicitly treating k-space data from adjacent slices as from different channels, and directly applying the strategies used in conventional parallel imaging. 1-mode unfolding is equivalent to treating k-space data from different slices as from different virtual channels. As revealed in traditional parallel imaging methods, each k-space sample can be linearly fitted with its neighborhood samples[2,16,28], and such linear dependency holds across the whole k-space. This leads to the low-

rankness of constructed block-wise Hankel matrix[16]. Additionally, each k-space sample can also be linearly fitted with the neighborhood samples in adjacent slices due to image content similarities among adjacent slices[8]. In this perspective, the matrix from 1-mode unfolding is more rank-deficient compared to the block-wise Hankel matrix constructed from single-slice k-space data (**Supporting Information Figure S1**). Second, the in-plane and through-plane spatial variation of coil sensitivity is extremely smooth, so that coil sensitivity maps (including their phase and magnitude) for adjacent slices are similar. Last, due to the slow spatial varying of the subject contour, different slices share similar spatial support. Therefore, the linear dependency not only holds across the whole k-space, but is also close among different slices. From this point of view, 2-mode unfolding, which is equivalent to treating data from different slices as from different virtual kernels, is also rank-deficient, with its rank close to that for single-slice block-wise Hankel matrix.

Multi-channel multi-slice reconstruction as low-rank tensor completion

Promoting low-rankness of the multi-slice tensor inherently exploits similarities among adjacent slices, including their similarities in coil sensitivity maps, spatial-support, and image content. On one hand, with low-rankness of 1-mode unfolding for multi-slice tensor promoted, each k-space sample can be interpolated from its neighborhood samples within a compact kernel. The neighborhood samples can be extracted from the same slice or adjacent slices, this forces adjacent slices to have smooth variation of anatomical structures along slice direction, i.e., similar image content across adjacent slices. On the other hand, promoting low-rankness of 2-mode unfolding for multi-slice tensor enforces the k-space samples within a compact kernel to be represented in a low dimensional subspace, and linear dependency of such subspace holds both within the whole k-space and across adjacent slices. This ensures that each k-space sample can be fitted with its neighborhood samples, and the fitting coefficients are similar across adjacent slices. Therefore, the coil sensitivity map and spatial-support of these slices should be similar.

A multi-slice tensor can be decomposed and approximated using rank truncation. In this study, high-order SVD (HOSVD) is used for tensor decomposition[26,30-32]. In literature, it is also called as multi-linear SVD[26] or Tucker decomposition[33]. HOSVD

decomposes the multi-slice tensor by computing a core tensor $\boldsymbol{S}$, and 3 orthonormal bases $U^{(n)}$ (n = 1, 2, and 3) for the 3 different subspaces of n-mode vectors[27],

$$\boldsymbol{T} = \boldsymbol{S} \times_1 U^{(1)} \times_2 U^{(2)} \times_3 U^{(3)} \quad (1)$$

Here $\times_n$ is the n-mode product of a tensor and a matrix, and $U^{(n)}$ is the unitary matrix, which can be obtained from SVD of the n-mode matrix unfolding $T_{(n)}$. Then, low-rank tensor approximation can be performed by hard thresholding the core tensor[31], or truncating the core tensor and unitary matrices when the n-mode ranks are known, which is similar to Cadzow algorithm used in SAKE reconstruction[16,34].

An updated k-space estimation can be generated from the low-rank approximated multi-slice tensor. Specifically, the multi-slice tensor entries corresponding to the same k-space sample are averaged and used as updated k-space estimation (structural consistency). After that, the difference between the estimated k-space and acquired data is minimized as below (data consistency). For Cartesian imaging, the data consistency is performed by simple substitution with the acquired data. For non-Cartesian imaging, the multi-slice tensor is also constructed from an estimated Cartesian k-space, which can be iteratively regenerated from the low-rank approximated multi-slice tensor. Non-uniform FFT (NUFFT)[35,36] builds the connection between acquired non-Cartesian data and the estimated Cartesian k-space. When enforcing data consistency for non-Cartesian imaging, the k-space data on non-Cartesian trajectories are calculated using NUFFT, and subtracted from the acquired data (Y). The difference is then mapped onto Cartesian grids using inverse NUFFT, and added to the current k-space estimation (X_n) (**Supporting Information Figure S2**). This can be written as,

$$X_{n+1} = X_n + D^{-1}(Y - DX_n) \quad (2)$$

where D denotes the sampling operator, D^{-1} is the gridding operation that maps non-Cartesian data onto Cartesian grids.

With n-mode ranks of multi-slice tensor known, the objective function can be formatted as

$$\underset{X}{argmin} \|DX - Y\|_F^2,$$

$$s.t.\ \boldsymbol{\Gamma} = \boldsymbol{S} \times_1 U^{(1)} \times_2 U^{(2)} \times_3 U^{(3)},$$

$$X = P^{-1}(\boldsymbol{\Gamma}) \quad (3)$$

where P is the operator that constructs multi-slice k-space data X into multi-slice tensor, P^{-1} is the reverse operator that generates k-space data from multi-slice tensor, $\boldsymbol{\Gamma}$ is a low-rank tensor of rank-(R_1, R_2, R_3), and $\|\cdot\|_F$ denotes the Frobenius norm. The implementation of our proposed calibrationless reconstruction using low-rank tensor completion consists of the following steps, as illustrated in **Figure 1**. First, multi-slice multi-channel k-space data are structured into a multi-slice tensor, which is decomposed and approximated as a low-rank tensor $\boldsymbol{\Gamma}$. In this work, sequentially truncated HOSVD (ST-HOSVD) is implemented for low rank tensor approximation, which converts the low rank approximation via matrix SVD and rank truncation of unitary matrices[37]. Specifically, ST-HOSVD approximates a low rank tensor by sequentially truncating the unitary matrices $U^{(n)}$. Matrix SVD algorithm is modified from a fast SVD implementation, which only computes a few singular values and eigenvectors[38]. The k-space is then recovered from the approximated tensor, with structural and data consistency applied. These steps are repeated to update the unacquired samples iteratively until convergence.

Multi-slice data acquisition and retrospective undersampling

The proposed method was evaluated with both non-Cartesian and Cartesian imaging. *In vivo* data were acquired on a 3T Phillips scanner equipped with an 8-channel head coil. All experiments involving human subjects were approved by the local institutional board and written information consent was obtained.

For 2D non-Cartesian spiral imaging, fully sampled data were acquired according to an 8-shot regular spiral trajectory, with acquisition window = 21 ms, TR/TE = 2700/54 ms, FOV = 220×220 mm^2, slice thickness/gap = 4/1 mm, matrix size = 220×220, slice number = 9, and spectral pre-saturation with inversion recovery (SPIR) used for fat suppression. The spiral interleaves spread evenly along azimuthal direction, and have the same rotation angle among adjacent slices. Undersampling was performed by discarding the spiral shots in an interleaved way. For different slices, the sampling complements each other by choosing the spiral shots with different rotation angles.

For 2D Cartesian imaging, both fully sampled T2w and T1w data were acquired. Data

for T2w imaging were acquired using a 15-shot multi-slice 2D fast spin echo (FSE) sequence, with echo train length (ETL) set to 24, TR/TE = 3000/115 ms, FOV = 240×240 mm^2, slice thickness/gap = 5/1 mm, matrix size = 360×360, slice number = 24, and phase-encoding along L/R direction. Data for T1w imaging were acquired using multi-slice 2D spin-echo (SE) sequence with TR/TE = 600/10 ms, flip angle = 70°, FOV = 240×240 mm^2, slice thickness/gap = 4/1 mm, matrix size = 240×240, slice number = 20, and phase-encoding along L/R direction. The k-space data were retrospectively undersampled by randomly discarding phase-encoding lines according to a 1-D Poisson disk pattern. The sampling pattern for different slices was generated independently, so that the remaining k-space data for different slices can provide complementary information.

Evaluation of the proposed method

The proposed method was compared to the traditional SAKE reconstruction, which is independently applied for single-slice data. The kernel size for both MS-HTC and SAKE was set to 6×6. For spiral imaging, NUFFT was performed using Kaiser-Bessel interpolator, with target image size = 220×220, neighborhood size = 6×6, and FFT size = 330×330.

The target rank was optimized for SAKE to ensure its best performance can be achieved. The optimized rank was also used as the target rank of 2-mode decomposition in MS-HTC reconstruction. As for 1-mode decomposition in MS-HTC, the target rank not only depends the coil sensitivity maps, spatial support, but is also related to their similarities among adjacent slices, and number of slices to be jointly reconstructed. In this study, target rank for 1-mode was empirically selected. The iteration process was stopped when the update of k-space data estimation is lower than 0.1‰.

To explore the performance of MS-HTC and SAKE with different kernel sizes, both methods were applied with kernel sizes of 3×3, 4×4, and 6×6 for the 8-channel T1w Cartesian data at R = 5. The influence of different thresholding ranks in MS-HTC and SAKE reconstruction was also demonstrated using the 8-channel T1w Cartesian data at R = 5. The target rank was optimized for both MS-HTC and SAKE. With 4-slice joint reconstruction using MS-HTC, the optimized rank was 1.25/1.61 for 1-mode/2-mode unfolding. The optimized rank was 1.61 for SAKE reconstruction for these 4

slices. For SAKE reconstruction, its performance with suboptimal rank selection was evaluated by deliberately setting a rank threshold much smaller/larger (1.11/3.61) than the optimized value. For MS-HTC, the rank of one mode was set deliberately made small/larger (0.75/3.25 for 1-mode unfolding, and 1.11/3.61 for 2-mode unfolding), while keeping the optimized rank for the other mode, such that the effects of each mode were independently evaluated.

The final image was generated by combining all coil images using square root sum-of-squares (rSOS) method. Besides visually comparing the results reconstructed from SAKE and MS-HTC, the residual error maps were calculated as the rSOS of the coil-by-coil difference between the reconstructed images and reference images reconstructed from fully sampled data. Root mean square error (RMSE) was calculated within the brain region for each slice.

Our proposed MS-HTC and its evaluation were implemented using MatLab (MathWorks, Natick, MA), and the source code can be obtained online (https://github.com/loyalliu/MS-HTC) or from the authors upon request.

Results

The results for T2w SE spiral imaging are shown in **Figure 2**. Fully sampled and four-fold undersampled data were directly reconstructed using NUFFT. MS-HTC jointly reconstructed these 4 slices, and SAKE reconstruction was performed on each slice independently. As depicted in **Figure 3**, these adjacent slices exhibited similar coil sensitivity maps in terms of their magnitude and phase. Note the coil sensitivity maps of these slices were calculated using ESPIRiT toolbox[39]. Direct NUFFT reconstruction from undersampled data with undersampling factor R = 4 suffered from severe aliasing artifacts in both brain and background regions. By comparing the aliasing pattern across adjacent slices, it could be clearly observed that the aliasing artifacts had different rotation angles, which corresponded to the rotation angles of the sampled spiral interleaves in adjacent slices. With SAKE reconstruction, artifacts in background region were significantly suppressed, while distinct artifacts were still present within the brain region. With MS-HTC, these artifacts were effectively eliminated in all slices.

Figure 4 compares the 4 consecutive slices from MS-HTC and SAKE reconstruction of Cartesian T2w FSE data at R = 4. For MS-HTC, these 4 slices were jointly reconstructed. For T2w FSE reconstruction, distinct artifacts exhibited in SAKE results (red arrow). With MS-HTC, these artifacts were effectively suppressed. As shown in error maps, MS-HTC results led to significantly reduced reconstruction error, with an overall ~20% reduction of RMSE compared to SAKE reconstruction.

As shown in **Figure 5**, for T1w imaging with SE, the improvement of MS-HTC over SAKE was even more significant because the slice thickness was smaller and the image content was more similar among adjacent slices. Pronounced artifacts were present in all 4 slices in SAKE results. They were absent in MS-HTC results, with error maps resembling noise-like patterns.

Figure 6 shows how number of jointly reconstructed slices influenced MS-HTC performance at different undersampling factors (R = 3, 4, and 5). Note that with relatively low undersampling (R = 3), increasing the number of slices did not necessarily improve the reconstruction performance. While at higher undersampling factors (R = 4, and 5), increasing slice number in MS-HTC reconstruction could further improve its performance in terms of residual artifacts and RMSE (**Figure 7**).

As shown in **Figure 8**, with an extremely compact kernel (3×3), MS-HTC exhibited slightly degraded reconstruction accuracy compared to that with larger kernel size. For SAKE reconstruction, the degradation became more pronounced and presented as increased artifact level. With a large kernel, the constructed multi-slice tensor (for MS-HTC) and single-slice matrix (for SAKE) become more rank-deficient (**Supporting Information Figure S3**), leading to improved reconstruction accuracy.

Figure 9A demonstrates the influence of different thresholding ranks in MS-HTC and SAKE reconstruction. For SAKE reconstruction, when the target rank was small, the image would present severe artifacts. For MS-HTC, if target rank for 1-mode unfolding was sufficiently small, there would be cross-talk among different slices, which was more distinct in the error maps. With target rank for 2-mode unfolding sufficiently small, MS-HTC also suffered from increased residual artifact, but it was significantly less compared to that in SAKE result (**Figure 9B**). This was probably because the information truncated in 2-mode unfolding could be partly recovered from the 1-mode

unfolding. With the target rank set to be too large in SAKE, the artifact would be very severe. For MS-HTC, with 1-mode rank set to be too large, the images would have increased artifact level and noise amplification. The results from MS-HTC with large 1-mode rank were similar to those from SAKE. This indicated that exploiting similarities in image content can significantly reduce this type of artifacts and suppress noise amplification due to high undersampling.

Discussion

Exploitation of multi-channel multi-slice information

The proposed MS-HTC jointly reconstructs multiple adjacent slices by simultaneously estimating the linear dependency among k-space samples and the missing samples through low-rank tensor completion. The existing calibrationless reconstruction approaches estimate linear dependency from undersampled k-space, and the estimation accuracy may be undermined if the k-space is highly undersampled, or sampling pattern does not provide sufficient incoherency. The degraded estimation of linear dependency can cause severe artifacts in reconstructed images. The proposed MS-HTC implicitly exploits the similarities among adjacent slices by promoting the low-rankness of 2-mode decomposition. In this regard, estimation of linear dependency is more accurate in MS-HTC reconstruction, leading to substantially reduced artifacts. Note that undersampling adjacent slices differently also enhances incoherence among adjacent slices in the wavelet domain[11,25]. Additional regularization can be applied to promote the sparsity in wavelet domain to further improve SNR.

When multiple adjacent slices are jointly reconstructed using MS-HTC, complementing the sampling pattern across adjacent slices can increase the incoherency, leading to significantly improved image quality. In this study, 1D Poisson disk sampling pattern was independently generated and applied for each slice in Cartesian imaging. This provides a uniform-density, yet random and complementary pattern for adjacent slices. In future studies, more efficient sampling schemes can be incorporated. For example, variable density sampling may provide better performance by more densely sampling the central k-space, where most k-space signal concentrates. In fact, Ahmad, et al.

proposed to use variable density incoherent spatiotemporal acquisition (VISTA) for highly accelerated cardiac cine MRI[40], where the highly incoherent spatial temporal sampling pattern produced diagnostic quality images at 15-fold acceleration. Variable density incoherent sampling pattern across different slices should also be valuable for further improving the image quality.

The proposed MS-HTC is more effective with spiral sampling trajectories than with Cartesian sampling trajectories. This is because spiral trajectory can provide a pseudo 2D undersampling pattern, which spreads the aliasing along both directions, leading to a noise-like pattern, especially when multiple shots are used. Choosing spiral interleaves with different angles for adjacent slices can make the sampling complement each other in a 2D manner, which can further enhance the performance of MS-HTC.

Parameter selection for the proposed method

In traditional GRAPPA, a larger kernel size usually leads to better performance, with the reconstructed images showing less artifacts and lower noise. This is because a larger kernel in k-space can better characterize the coil sensitivity variation in image-space, and the SNR of the reconstructed images will be closer to that from image-space reconstruction (e.g. SENSE) with accurate coil sensitivity calibration. In iterative k-space reconstruction (e.g., SPIRiT), the reconstruction is less sensitive to the kernel size, but using a larger kernel still slightly increases reconstruction accuracy in terms of residual artifacts and noise. Our proposed MS-HTC performs parallel imaging reconstruction by finding a low-dimensional subspace for the constructed tensor, and a larger kernel size leads to a more rank-deficient multi-slice tensor (**Supporting Information Figure S3**), thus providing improved reconstruction accuracy. Note that, in all aforementioned methods, larger kernel size also increases the reconstruction time. Therefore, a kernel size that can provide sufficient reconstruction accuracy should be used.

As in single-slice reconstruction using SAKE, the rank of the constructed matrix is determined by many factors, including the coil number/configuration, kernel size, and spatial support of the object within the FOV[16]. For MS-HTC, the optimal rank is also related to number of jointly reconstructed slices, and their similarities in coil sensitivity maps and image content. Increased similarities across consecutive slices can lower the

rank of the constructed tensor. In this study, the target rank is empirically determined, but may not be easily obtained in practice when ground truth is not available. Automatically determining the target rank or circumventing the inconvenient rank selection problem via a singular value shrinkage scheme can be investigated in future studies[22,38,41,42].

As revealed in **Figure 9**, promoting low-rankness of 1-mode and 2-mode exploits different types of data redundancies for multi-channel multi-slice data. Promoting low-rankness of 1-mode unfolding utilizes the similarity of image content across adjacent slices, while promoting the low-rankness of 2-mode unfolding utilizes the similarity of coil sensitivity and spatial support of adjacent slices. Careful adjustment of the target rank of different modes unfolding can provide a balance between the exploitation of image content similarity and coil sensitivity/spatial-support similarity.

With increased number of jointly reconstructed slices, the constructed tensor becomes more rank-deficient (**Supporting Information Figure S1**), which can lead to further improved reconstruction, as shown in **Figure 6**. Note that as slice gap increases, the decreased similarities can undermine the performance of MS-HTC. As shown in **Supporting Information Figure S4**, though the overall image quality of MS-HTC results was still better compared to that of SAKE results, it was degraded compared to MS-HTC results with small slice gap (**Figure 4**). This was expected due to the decrease of similarities in coil sensitivity maps and image content. Note that, in presence of air-tissue boundaries, the coil sensitivity and image content may also change dramatically, especially at ultra-high field systems. In such scenarios, reconstruction with fewer slices or with increased target rank can be used to improve the performance.

Computation efficiency of the proposed method

In our implementation, we used a personal desktop computer (PC) equipped with 4-core i5-6500 CPU and 16-GB RAM, and ran the reconstruction on MATLAB 2016b. For 8-channel T1w data with matrix size = 240×240 and R = 3. The kernel size was set to 6×6 for MS-HTC and SAKE. The reconstruction times were summarized in **Table 1**. The overall reconstruction speed for MS-HTC with different number of jointly reconstructed slices were similar.

For both MS-HTC and SAKE, the most time-consuming procedures are tensor/matrix decomposition, block-wise Hankel tensor/matrix construction from k-space data, and k-space data generation from block-wise tensor/matrix. The reconstruction time will increase dramatically as the k-space data matrix size and kernel size increase. In practice, the computational time can be reduced by increasing the convergence rate, reducing the computation cost of each iteration, or/and using GPU-based parallel computation.

Similar to SAKE, the proposed MS-HTC simultaneously estimates the linear dependency and missing k-space data, and the convergence rate can be very slow if the central k-space is also sparse. Strategies including successive over-relaxation[43], scheduled relaxation[44] that uses a lager relaxation factor to update the k-space data by promoting the low-rankness of multi-slice tensor.

Low-rankness can also be enforced on multi-slice tensor constructed from partial k-space, which is conceptually similar to ordered subset expectation maximization (OS-EM) for PET/SPECT reconstruction[45] or stochastic gradient descent (SGD) for model training in machine learning[46]. This strategy may significantly reduce computation time of each iteration, achieve much faster convergence, and require less memory consumption.

Future studies may also include developing the heavy computational algorithms with GPU-based acceleration, e.g., developing in MATLAB with Jacket (a GPU engine for MATLAB)[47] or C++ with NVIDIA CUDA extension. Such approaches can potentially achieve near real-time reconstruction.

Conclusion

Our proposed MS-HTC approach exploits the similar coil sensitivity and image content within adjacent multi-slice MR data through a tensor completion framework. It offers a new and effective approach to acquire and reconstruct highly undersampled multi-slice multi-channel MR data in a calibrationless manner.

Acknowledgments

This study is supported in part by Hong Kong Research Grant Council (R7003-19 and C7048-16G to E.X.W. and HKU17103819 to A.T.L.), Guangdong Key Technologies for Treatment of Brain Disorders (2018B030332001 to E.X.W.), and Guangdong-Hong Kong-Macao Greater Bay Area Center for Brain Science and Brain-Inspired Intelligence Fund (2019008) and HKU Seed Fund for Basic Research (104005866 to A.T.L.) .

Reference

[1] Pruessmann KP, Weiger M, Scheidegger MB, Boesiger P. SENSE: sensitivity encoding for fast MRI. Magn Reson Med 1999;42(5):952-962.

[2] Griswold MA, Jakob PM, Heidemann RM *et al*. Generalized autocalibrating partially parallel acquisitions (GRAPPA). Magn Reson Med 2002;47(6):1202-1210.

[3] Atkinson D, Larkman DJ, Batchelor PG, Hill DL, Hajnal JV. Coil-based artifact reduction. Magn Reson Med 2004;52(4):825-830.

[4] Xie VB, Lyu M, Liu Y, Feng Y, Wu EX. Robust EPI Nyquist ghost removal by incorporating phase error correction with sensitivity encoding (PEC-SENSE). Magn Reson Med 2018;79(2):943-951.

[5] Blaimer M, Breuer F, Mueller M *et al*. SMASH, SENSE, PILS, GRAPPA: how to choose the optimal method. Top Magn Reson Imaging 2004;15(4):223–236.

[6] Polimeni JR, Bhat H, Witzel T *et al*. Reducing sensitivity losses due to respiration and motion in accelerated echo planar imaging by reordering the autocalibration data acquisition. Magn Reson Med 2016;75(2):665-679.

[7] Weizman L, Rahamim O, Dekel R, Eldar YC, Ben-Bashat D. Exploiting similarity in adjacent slices for compressed sensing MRI. Conf Proc IEEE Eng Med Biol Soc 2014;2014:1549-1552.

[8] Pang Y, Zhang X. Interpolated compressed sensing for 2D multiple slice fast MR imaging. PLoS One 2013;8(2):e56098.

[9] Datta S, Deka B. Magnetic resonance image reconstruction using fast interpolated compressed sensing. Journal of Optics-India 2018;47(2):154-165.

[10] Datta S, Deka B. Efficient interpolated compressed sensing reconstruction scheme for 3D MRI. IET Image Processing 2018;12(11):2119-2127.

[11] Lustig M, Donoho D, Pauly JM. Sparse MRI: The application of compressed sensing for rapid MR imaging. Magn Reson Med 2007;58(6):1182-1195.

[12] Liu Y, Cao J, Lyu M, Wu EX. Calibrationless parallel imaging reconstruction using Hankel tensor completion (HTC). In: 25th Annual Meeting of ISMRM, Honolulu, 2017, p 0445.

[13] Honal M, Bauer S, Ludwig U, Leupold J. Increasing efficiency of parallel imaging for 2D multislice acquisitions. Magn Reson Med 2009;61(6):1459-1470.

[14] Honal M, Leupold J, Huff S, Baumann T, Ludwig U. Compensation of breathing motion artifacts for MRI with continuously moving table. Magn Reson Med 2010;63(3):701-712.

[15] Breuer FA, Kellman P, Griswold MA, Jakob PM. Dynamic autocalibrated parallel imaging using temporal GRAPPA (TGRAPPA). Magn Reson Med 2005;53(4):981-985.

[16] Shin PJ, Larson PE, Ohliger MA *et al*. Calibrationless parallel imaging reconstruction based on structured low-rank matrix completion. Magn Reson Med 2014;72(4):959-970.

[17] Haldar JP. Low-Rank Modeling of Local-Space Neighborhoods (LORAKS) for Constrained MRI. IEEE Trans Med Imaging 2014;33(3):668-681.

[18] Haldar JP, Zhuo J. P-LORAKS: Low-rank modeling of local k-space neighborhoods with parallel imaging data. Magn Reson Med 2016;75(4):1499-1514.

[19] Lee J, Jin KH, Ye JC. Reference-free single-pass EPI Nyquist ghost correction using annihilating filter-based low rank Hankel matrix (ALOHA). Magn Reson Med 2016;76(6):1775-1789.

[20] Lee D, Jin KH, Kim EY, Park SH, Ye JC. Acceleration of MR parameter mapping using annihilating filter-based low rank hankel matrix (ALOHA). Magn Reson Med 2016;76(6):1848-1864.

[21] Lyu M, Barth M, Xie VB *et al*. Robust SENSE reconstruction of simultaneous multislice EPI with low-rank enhanced coil sensitivity calibration and slice-dependent 2D Nyquist ghost correction. Magn Reson Med 2018;80(4):1376-1390.

[22] Liu Y, Lyu M, Barth M *et al*. PEC-GRAPPA reconstruction of simultaneous multislice EPI with slice-dependent 2D Nyquist ghost correction. Magn Reson Med 2019;81(3):1924-1934.

[23] Lobos RA, Javed A, Nayak KS, Hoge WS, Haldar JP. Robust Autocalibrated Loraks for Epi Ghost Correction. Proc IEEE Int Symp Biomed Imaging 2018;2018:663-666.

[24] Datta S, Deka B, Mullah HU, Kumar S. An efficient interpolated compressed sensing method for highly correlated 2D multi-slice MRI. In: 2016 International Conference on Accessibility to Digital World (ICADW), Guwahati, 2016, p 187-192.

[25] Lustig M, Donoho DL, Pauly JM. Multi-slice compressed sensing imaging. In: 15th Annual Meeting of ISMRM, Berlin, 2007, p 828.

[26] De Lathauwer L, De Moor B, Vandewalle J. A Multilinear Singular Value Decomposition. Siam Journal on Matrix Analysis and Applications 2000;21(4):1253-1278.

[27] Trzasko JD, Manduca A. A unified tensor regression framework for calibrationless dynamic, multi-channel MRI reconstruction. In: 21st Annual Meeting of ISMRM, Salt Lake City, 2013, p 603.

[28] Lustig M, Pauly JM. SPIRiT: Iterative self-consistent parallel imaging reconstruction from arbitrary k-space. Magn Reson Med 2010;64(2):457-471.

[29] Deka B, Datta S. Calibrationless joint compressed sensing reconstruction for rapid parallel MRI. Biomedical Signal Processing and Control 2020;58:101871.

[30] Yi Z, Liu Y, Zhao Y, Chen F, Wu EX. Joint calibrationless reconstruction of highly undersampled multi-contrast MR datasets using a novel low-rank completion approach. In: 27th Annual Meeting of ISMRM, Montreal, 2019, p 4746.

[31] Zhang XY, Peng J, Xu M *et al*. Denoise diffusion-weighted images using higher-order singular value decomposition. Neuroimage 2017;156:128-145.

[32] Yu Y, Jin J, Liu F, Crozier S. Multidimensional compressed sensing MRI using tensor decomposition-based sparsifying transform. PLoS One 2014;9(6):e98441.

[33] Tucker LR. Some mathematical notes on three-mode factor analysis. Psychometrika 1966;31(3):279-311.

[34] Chu MT, Funderlic RE, Plemmons RJ. Structured low rank approximation. Linear Algebra and its Applications 2003;366:157-172.

[35] Fessler JA. On NUFFT-based gridding for non-Cartesian MRI. J Magn Reson 2007;188(2):191-195.

[36] Fessler JA, Sutton BP. Nonuniform fast Fourier transforms using min-max interpolation. IEEE Transactions on Signal Processing 2003;51(2):560-574.

[37] Vannieuwenhoven N, Vandebril R, Meerbergen K. A New Truncation Strategy for the Higher-Order Singular Value Decomposition. SIAM Journal on Scientific Computing 2012;34(2):A1027-A1052.

[38] Lingala SG, Hu Y, DiBella E, Jacob M. Accelerated dynamic MRI exploiting sparsity and low-rank structure: k-t SLR. IEEE Trans Med Imaging 2011;30(5):1042-1054.

[39] Uecker M, Lai P, Murphy MJ *et al*. ESPIRiT--an eigenvalue approach to autocalibrating parallel MRI: where SENSE meets GRAPPA. Magn Reson Med 2014;71(3):990-1001.

[40] Ahmad R, Xue H, Giri S *et al*. Variable density incoherent spatiotemporal acquisition (VISTA) for highly accelerated cardiac MRI. Magn Reson Med 2015;74(5):1266-1278.

[41] Majumdar A, Ward RK. An algorithm for sparse MRI reconstruction by Schatten p-norm minimization. Magn Reson Imaging 2011;29(3):408-417.

[42] Miao X, Lingala SG, Guo Y *et al*. Accelerated cardiac cine MRI using locally low rank and finite difference constraints. Magn Reson Imaging

2016;34(6):707-714.

[43] Hadjidimos A. Successive overrelaxation (SOR) and related methods. Journal of Computational and Applied Mathematics 2000;123(1-2):177-199.

[44] Yang XIA, Mittal R. Acceleration of the Jacobi iterative method by factors exceeding 100 using scheduled relaxation. Journal of Computational Physics 2014;274:695-708.

[45] Hudson HM, Larkin RS. Accelerated image reconstruction using ordered subsets of projection data. IEEE Trans Med Imaging 1994;13(4):601-609.

[46] Bottou L. Large-Scale Machine Learning with Stochastic Gradient Descent. Compstat'2010: 19th International Conference on Computational Statistics 2010:177-186.

[47] Larsen T, Pryor G, Malcolm J. Jacket: GPU Powered MATLAB Acceleration. In: Hwu W-mW, editor. GPU Computing Gems. Jade ed. Waltham, USA: Elsevier; 2012. p 387-398.

Table 1. Reconstruction time for MS-HTC and SAKE

	MS-HTC			SAKE
	2 slices	3 slices	4 slices	
Iteration number	193	192	145	352
Reconstruction time (second per slice)	453	473	380	336

Figure Captions

Figure 1. Diagram of joint multi-slice reconstruction with block-wise Hankel tensor completion (MS-HTC). Within each iteration, (1) multi-slice datasets are constructed into a 3rd-order tensor, where block-wise Hankel matrices constructed for multiple slices are concatenated along the 3rd dimension. (2) HOSVD is then applied to decompose the constructed multi-slice tensor into multiplication of a core tensor S and unitary matrices $U^{(1)}$, $U^{(2)}$, and $U^{(3)}$. (3) Low-rank approximation is performed through multilinear low-rank representation of $U^{(1)}$, $U^{(2)}$, $U^{(3)}$, and S, and the unacquired data are updated by exploiting multi-slice correlations and redundancies. (4) Last, k-space is recovered from the low-rank tensor, imposing the data consistency by minimizing the difference between estimated k-space and acquired data, and structural consistency by enforcing the multi-slice tensor entries from the same k-space sample to be identical.

Figure 2. Reconstruction for 8-channel T2w SE spiral data. (A) Reference images reconstructed from 8 shots using NUFFT. (B) Images reconstructed from 2 shots using NUFFT, MS-HTC, and SAKE. (C) Error maps displayed with enhanced brightness (×5) and root mean square error (RMSE) calculated within brain region for each slice. The results show that compared to SAKE, MS-HTC could have significantly reduced artifacts and noise amplification.

Figure 3. (A) Magnitude and (B) phase of coil sensitivity maps corresponding to the 4 consecutive slices displayed in Figure 2A. Each row includes the coil sensitivity maps of a selected coil for those consecutive slices. The coil sensitivity maps were calculated using ESPIRiT toolbox. Note that the coil sensitivity maps for adjacent slices show similar and smooth magnitude and phase distribution.

Figure 4. Reconstruction for 8-channel Cartesian T2w FSE data. Retrospective undersampling was performed by randomly discarding phase-encoding lines following a 1D Poisson disk pattern. (A) Fully sampled data were reconstructed and used as reference, and undersampled data were reconstructed with MS-HTC or SAKE. (B) The error maps for MS-HTC or SAKE were displayed with enhanced brightness.

Figure 5. Reconstruction for 8-channel Cartesian T1w SE data. Retrospective undersampling was performed by randomly discarding phase-encoding lines following

a 1D Poisson disk pattern. (A) Fully sampled data were reconstructed and used as reference, and undersampled data were reconstructed with MS-HTC or SAKE. (B) The error maps for MS-HTC or SAKE are displayed with enhanced brightness.

Figure 6. Evaluation of MS-HTC with different number of jointly reconstructed slices. (A) Reconstruction for 8-channel T2w Cartesian data undersampled with 1D Poisson disk at R = 2-4. For MS-HTC, data corresponding to 2 (Slice I-II), 3 (Slice I-III), or 4 (Slice I-IV) consecutive slices shown in Figure 4 were jointly reconstructed. Only Slice II is displayed. (B) Reconstruction for 8-channel undersampled spiral data. For MS-HTC, data corresponding to 2 (Slice I-II), 3 (Slice I-III), or 4 (Slice I-IV) consecutive slices shown in Figure 2 were jointly reconstructed. Only Slice II is displayed. Results show that MS-HTC could significantly reduce residual artifacts, especially at higher acceleration factors (R = 4).

Figure 7. Error maps corresponding to Figure 6. When selected slices were sufficiently similar in terms of coil sensitivity and image content, with increased number of jointly reconstructed slices, the MS-HTC further reduced reconstruction error in terms of residual artifacts and RMSE.

Figure 8. Reconstructed images and error maps (brightness × 5) for MS-HTC and SAKE with different kernel sizes for 8-channel T1w Cartesian data undersampled at R = 5.

Figure 9. Reconstruction for 8-channel T1w Cartesian data undersampled at R = 5. (**A**) Results for MS-HTC and SAKE with suboptimal rank. The error maps are displayed with enhanced brightness (×5). (**B**) Reconstructed images for fully sampled reference, and MS-HTC/ SAKE with optimized target rank.

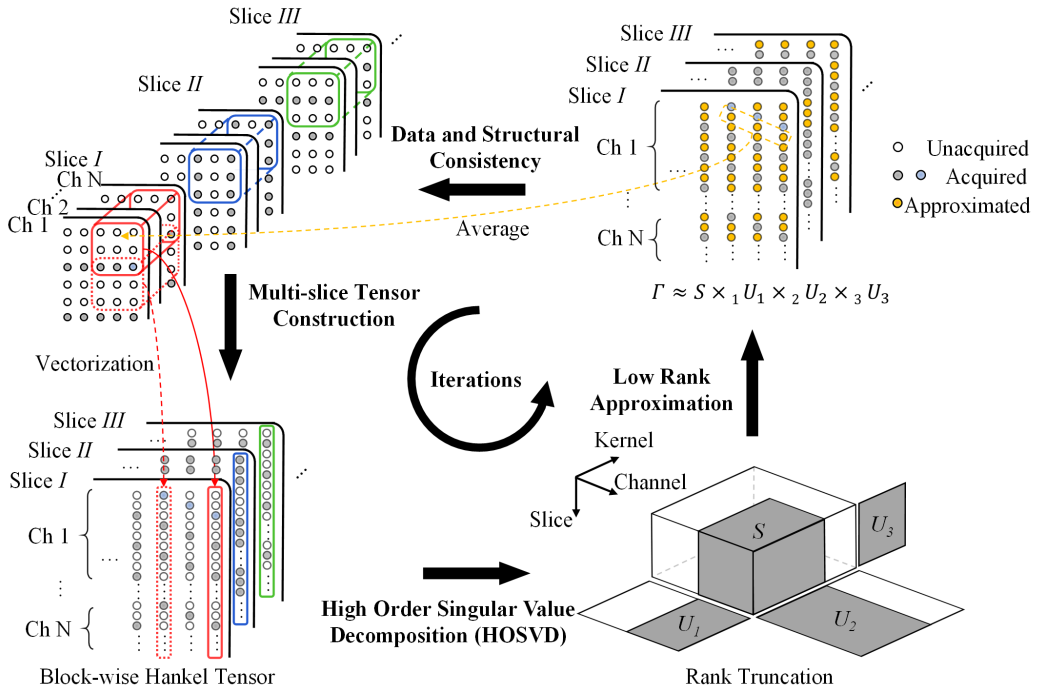

Figure 1

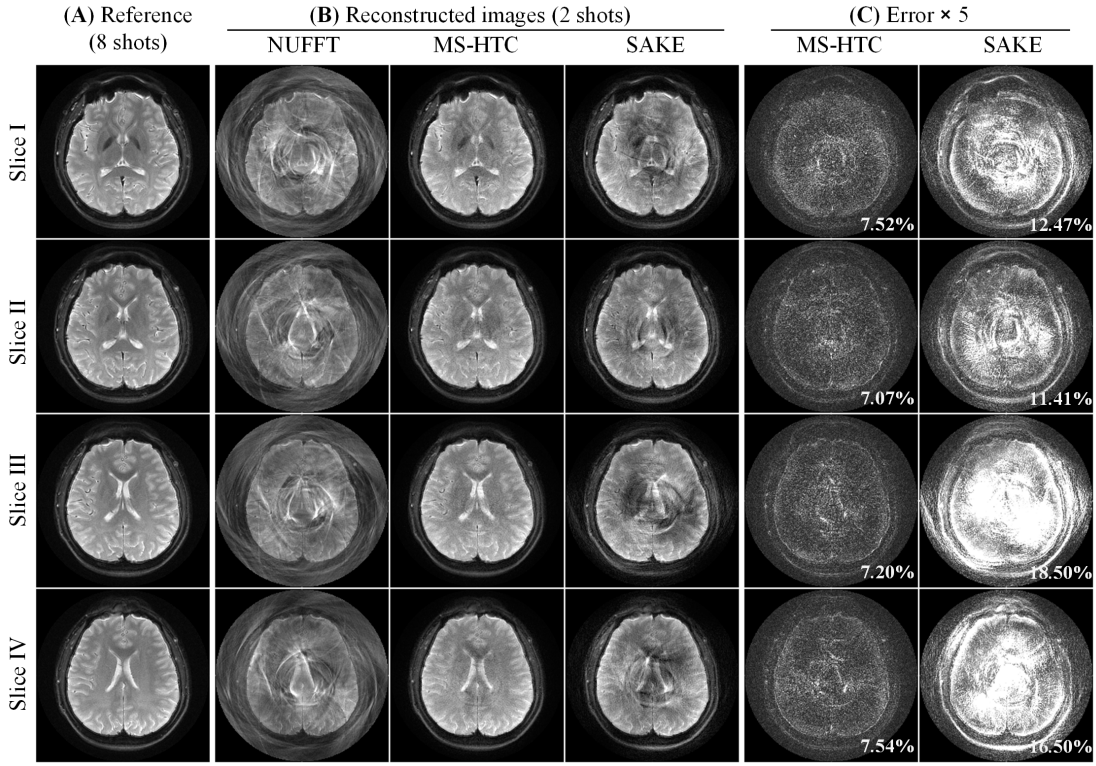

Figure 2

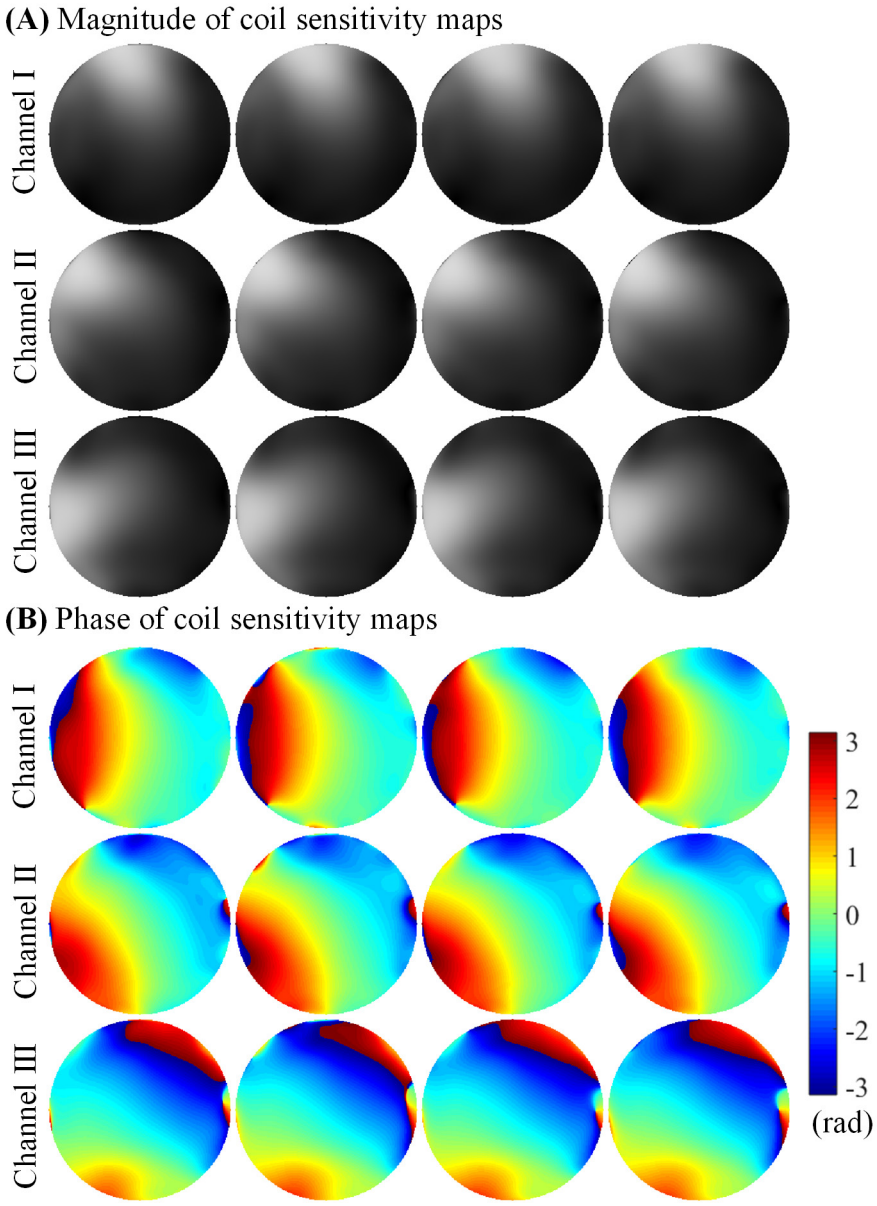
(A) Magnitude of coil sensitivity maps
Channel I
Channel II
Channel III
(B) Phase of coil sensitivity maps
Channel I
Channel II
Channel III
3
2
1
0
-1
-2
-3
(rad)

Figure 3

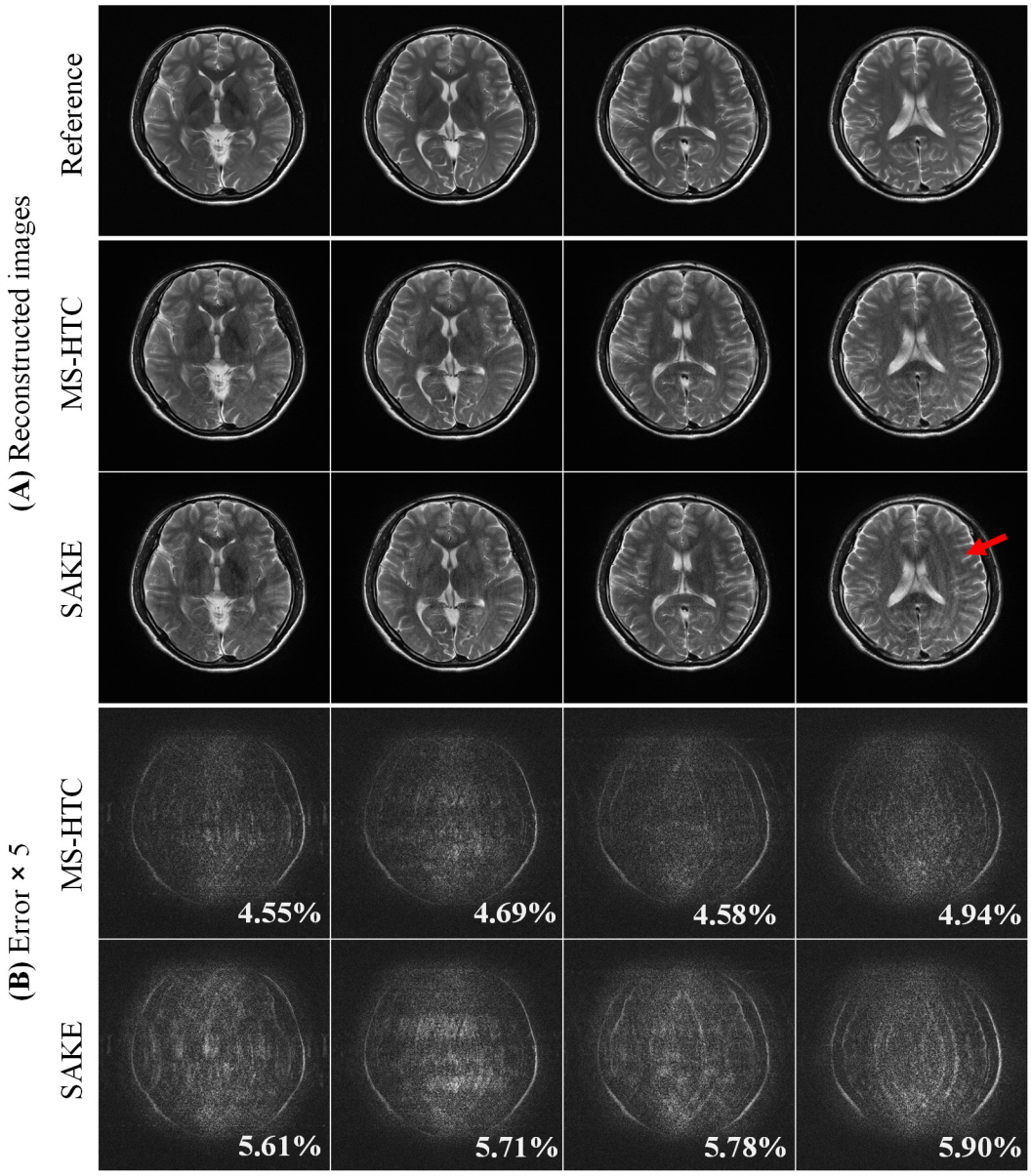
(A) Reconstructed images
Reference
MS-HTC
SAKE
(B) Error × 5
MS-HTC
SAKE
4.55%
4.69%
4.58%
4.94%
5.61%
5.71%
5.78%
5.90%

Figure 4

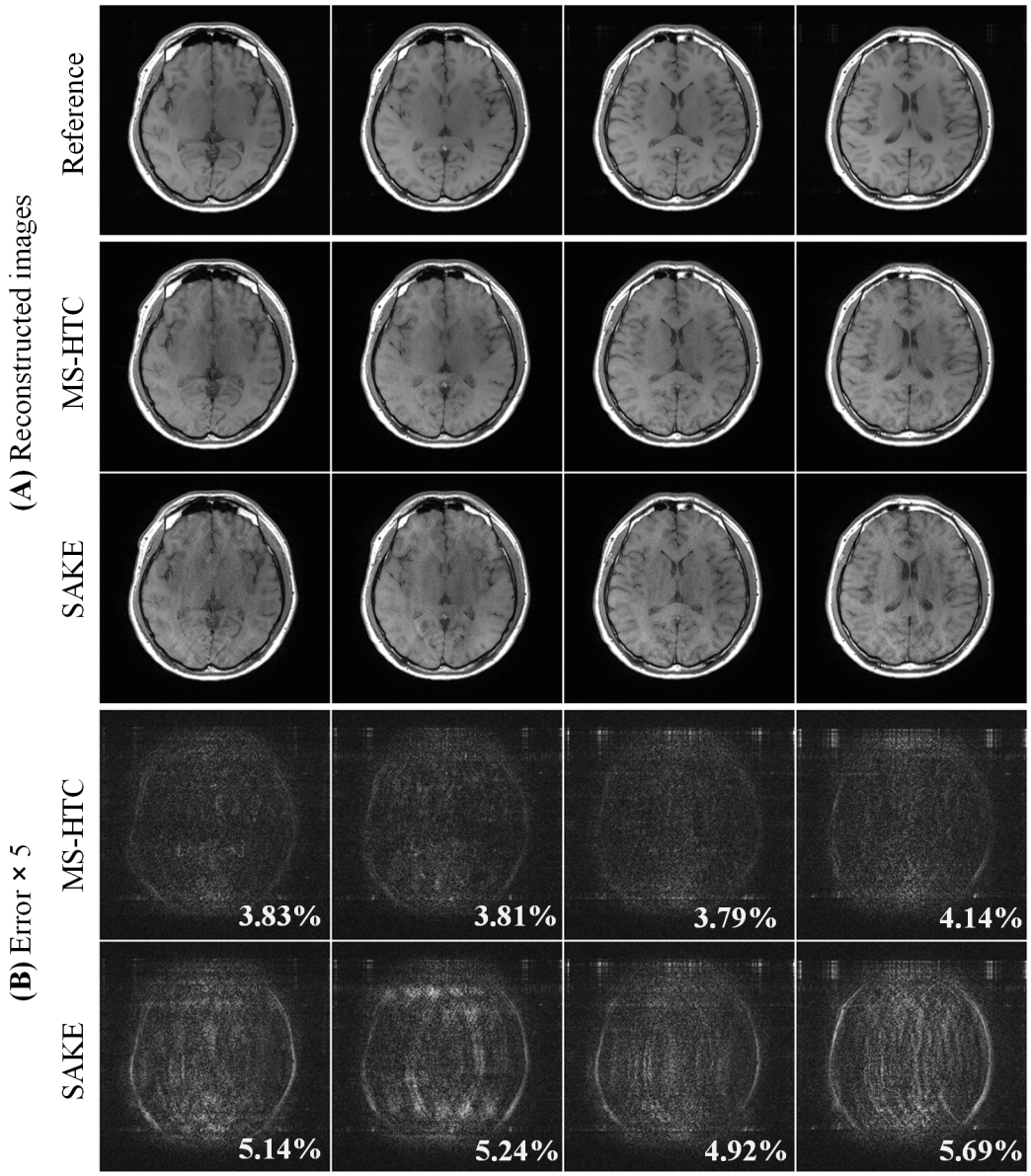
(A) Reconstructed images
Reference
MS-HTC
SAKE
(B) Error × 5
MS-HTC
SAKE
3.83%
3.81%
3.79%
4.14%
5.14%
5.24%
4.92%
5.69%

Figure 5

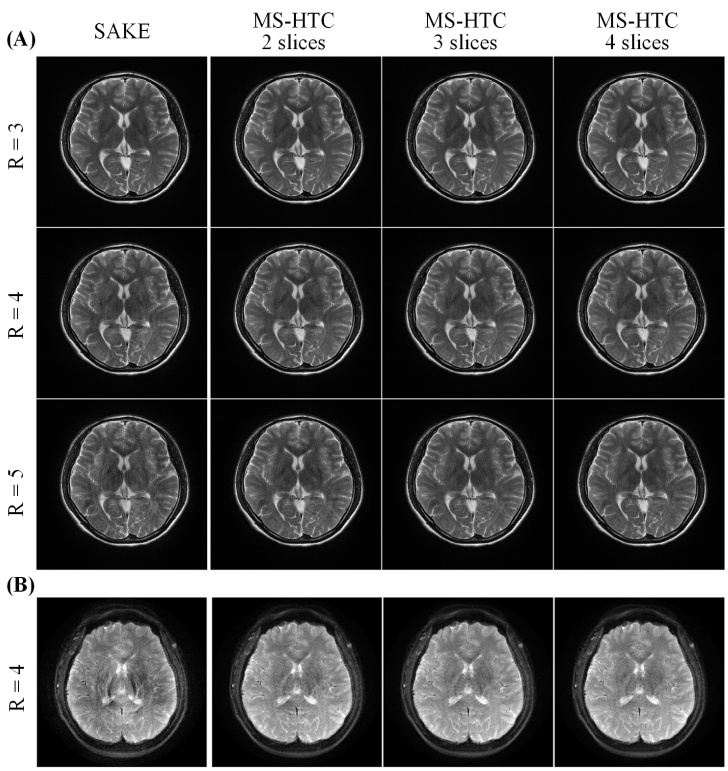

Figure 6

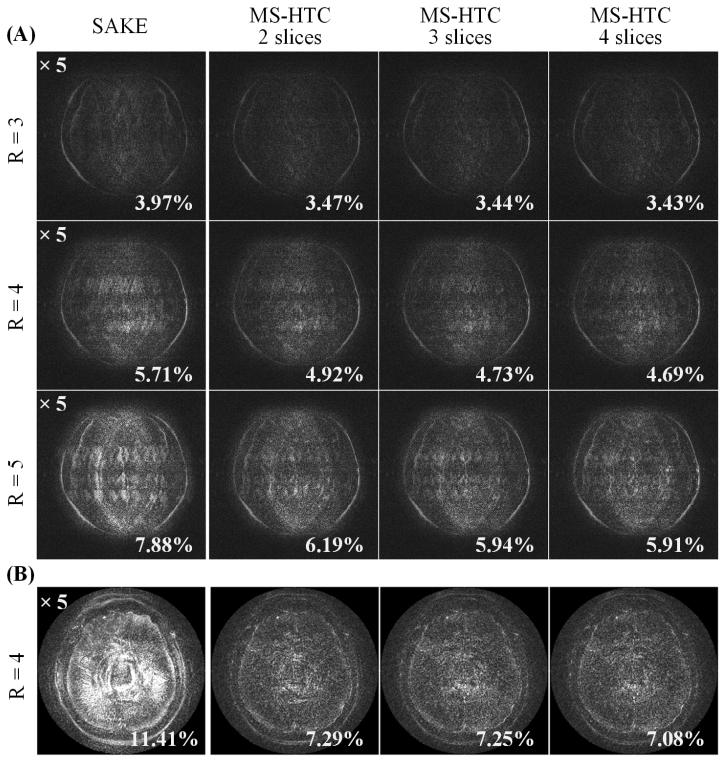

Figure 7

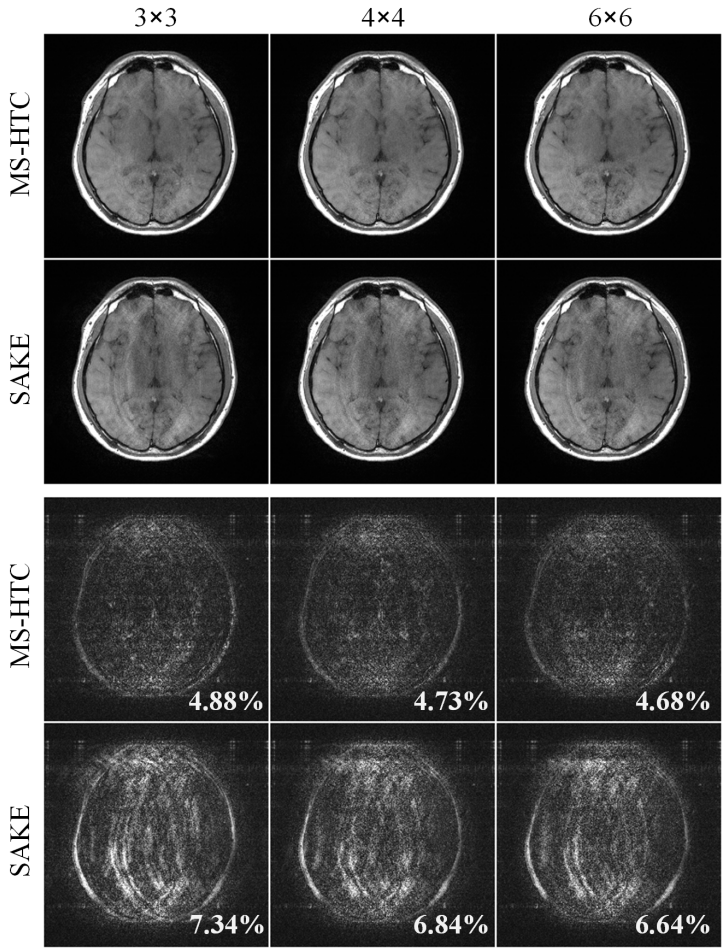

Figure 8

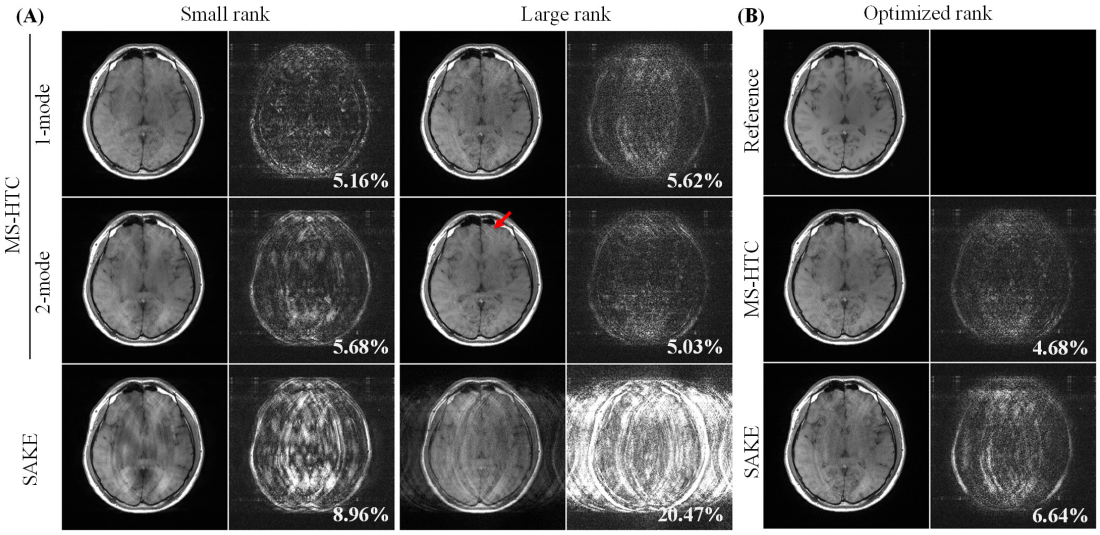

Figure 10